Cellular and Molecular Neurobiology (2019) 39:223–240
https://doi.org/10.1007/s10571-018-0642-1

ORIGINAL RESEARCH

miR-9 Upregulation Integrates Post-ischemic Neuronal Survival and Regeneration In Vitro

Sreekala S. Nampoothiri[1] · G. K. Rajanikant[1]

Received: 22 September 2018 / Accepted: 7 December 2018 / Published online: 11 December 2018

Abstract

The irrefutable change in the expression of brain-enriched microRNAs (miRNAs) following ischemic stroke has promoted the development of radical miRNA-based therapeutics encompassing neuroprotection and neuronal restoration. Our previous report on the systems-level prediction of miR-9 in post-stroke-induced neurogenesis served as a premise to experimentally uncover the functional role of miR-9 in post-ischemic neuronal survival and regeneration. The oxygen-glucose deprivation (OGD) in SH-SY5Y cells significantly reduced miR-9 expression, while miR-9 mimic transfection enhanced post-ischemic neuronal cell viability. The next major objective involved the execution of a drug repositioning strategy to augment miR-9 expression via structure-based screening of Food and Drug Administration (FDA)-approved drugs that bind to Histone Deacetylase 4 (HDAC4), a known miR-9 target. Glucosamine emerged as the top hit and its binding potential to HDAC4 was verified by Molecular Dynamics (MD) Simulation, Drug Affinity Responsive Target Stability (DARTS) assay, and MALDI-TOF MS. It was intriguing that the glucosamine treatment 1-h post-OGD was associated with the increased miR-9 level as well as enhanced neuronal viability. miR-9 mimic or post-OGD glucosamine treatment significantly increased the cellular proliferation (BrdU assay), while the neurite outgrowth assay displayed elongated neurites. The enhanced BCL2 and VEGF parallel with the reduced NFκB1, TNF-α, IL-1β, and iNOS mRNA levels in miR-9 mimic or glucosamine-treated cells further substantiated their post-ischemic neuroprotective and regenerative efficacy. Hence, this study unleashes a potential therapeutic approach that integrates neuronal survival and regeneration via small-molecule-based regulation of miR-9 favoring long-term recovery against ischemic stroke.

Keywords MiRNA-9 · HDAC4 · Glucosamine · Ischemic stroke · Neuron regeneration · Proliferation · Neuroprotection · Drug repurposing

Abbreviations

ANOVA	Analysis of variance
ATP	Adenosine triphosphate
BCL2	B-cell lymphoma 2
BrdU	5-Bromo-2´-deoxyuridine
DARTS	Drug affinity responsive target stability
DMEM	Dulbecco's modified Eagle's medium
EBSS	Earle's balanced salt solution
FBS	Fetal bovine serum
FDA	Food and drug administration
GAPDH	Glyceraldehyde 3-phosphate dehydrogenase
HDAC4	Histone deacetylase-4
IL-1β	Interleukin-1β
iNOS	Inducible nitric oxide synthase
LDH	Lactate dehydrogenase
MALDI-TOF MS	Matrix-assisted laser desorption/ionization - time-of-flight mass spectrometry
MD	Molecular dynamics
MTT	3-(4,5-dimethylthiazol-2-yl)-2,5-diphenyltetrazolium bromide
NFκB1	Nuclear Factor Kappa B Subunit 1
OGD	Oxygen-glucose deprivation
PBS	Phosphate-buffered saline
PDB	Protein data bank

Electronic supplementary material The online version of this article (https://doi.org/10.1007/s10571-018-0642-1) contains supplementary material, which is available to authorized users.

✉ G. K. Rajanikant
rajanikant@nitc.ac.in

[1] School of Biotechnology, National Institute of Technology Calicut, Calicut 673601, India

PI	Propidium iodide
qRT-PCR	Quantitative real time-polymerase chain reaction
RMSD	Root-mean-square deviation
RMSF	Root-mean-square fluctuation
SDS	Sodium dodecyl sulfate
SDS–PAGE	Sodium dodecyl sulfate–polyacrylamide gel electrophoresis
SEM	Standard error of the mean
TNF-α	Tumor necrosis factor-α
VEGF	Vascular endothelial growth factor

Introduction

Specific brain-enriched miRNAs fine-tune neurogenic processes regulating neuronal proliferation and differentiation (Shen and Temple 2009; Shi et al. 2010; Lang and Shi 2012; Nampoothiri and Rajanikant 2017). Modulating the activity of these miRNAs may have therapeutic relevance in ischemic stroke (Khoshnam et al. 2017; Ouyang et al. 2013; Nampoothiri et al. 2016). Of late, there has been a paradigm shift from neuroprotective to neuronal restoration miRNA-based strategies that promote long-term post-stroke recovery (Cramer 2018; Liu et al. 2011, 2013a, b). Given the rising interest in miRNA-mediated neuronal repair, our recently published study delved into the miRNA-regulatory network in ischemic stroke and predicted the association of miR-9 and histone deacetylase-4 (HDAC4) in post-stroke-induced neurogenesis (Nampoothiri et al. 2018). Therefore, we hypothesized that integration of neuronal survival and regeneration by regulating miR-9 expression would be appealing as a radical approach for the treatment of ischemic stroke.

miR-9 exhibits a distinct expression pattern in the brain and orchestrates processes involved in the development of the central nervous system (Coolen et al. 2013). It is essential for embryonic and adult neuronal progenitor cell differentiation and maintenance (Zhao et al. 2009). miR-9 negatively regulates HDAC4, stabilizing its expression through a positive feedback mechanism and enhances the neurogenic potential of neural precursor cells (Davila et al. 2014). A few previous reports suggest the neuroprotective role of miR-9 in cerebral ischemia (Wei et al. 2016; Chen et al. 2017); however, there has been a limited insight into the function of miR-9 in neuronal regeneration post-ischemia.

The current study was conceptualized to delineate the role of miR-9 in post-ischemic neuron regeneration and survival. The miR-9 expression was quantified with the subsequent assessment of miR-9 upregulation on neuronal viability and neurite outgrowth in an *in-vitro* model for ischemic stroke. The study was further extended wherein computational drug repositioning approach was implemented to identify a suitable pharmacological intervention targeting HDAC4 (a class IIa specific HDAC and a known miR-9 target) likely to act as an alternative for the exogenous administration of miR-9 mimic. To the best of our knowledge, this is the first study that unravels the significance of miR-9 upregulation in integrating post-ischemic neuronal regeneration and survival.

Methodology

Transient Transfection of SH-SY5Y Cells with miRNA-9

SH-SY5Y cells were procured from National Centre for Cell Science, Pune, India, and cultured as previously described (Davis et al. 2018). The cells were transiently transfected with miR-9-5p mimic (Eurogentec, Belgium), miR-9-5p inhibitor (Thermo Fisher Scientific, MA, USA), and the corresponding negative controls (mirVana™ miRNA Mimic Negative Control #1 and mirVana™ miRNA Inhibitor, Negative Control #1) (Thermo Fisher Scientific, MA, USA) using Invitrogen™ Lipofectamine™ RNAiMAX transfection reagent (Thermo Fisher Scientific, MA, USA) according to the manufacturer's instructions. The transfection mixture was prepared in Opti-MEM™ reduced serum medium (Thermo Fisher Scientific, MA, USA). The cells were incubated with the corresponding miRNA-lipid complex for 10 h. An optimized final concentration of 50 nM was used for miR-9 mimic, inhibitor, and the negative controls.

Oxygen-Glucose Deprivation (OGD)

SH-SY5Y cells were exposed to OGD by replacing the culture medium with Earle's balanced salt solution (EBSS) (Thermo Fisher Scientific, MA, USA), and the cells were placed in modular incubator chamber (Billups-Rothenberg, Del Mar, USA). The chamber was sealed and flushed with a mixture of 95% N_2 and 5% CO_2 for 5 min with a flow rate of 40 L/min. Both the ports were sealed, and the chamber was kept in an incubator at 37 °C for 2 h. OGD was terminated by replacing the EBSS with DMEM/F12 medium containing 10% FBS. The culture was then placed in the incubator for reoxygenation (OGD/R). The control cells were untreated and maintained under normoxic condition (5% CO_2 and 95% air) with DMEM/F12 containing 10% FBS.

miRNA Isolation and miR-9 Expression Analysis

SH-SY5Y cells were seeded in a 6-well plate at a density of 3×10^5 cells/well. Total RNA was extracted from the harvested cells at 4-h and 20-h post-OGD using mirVana™ miRNA Isolation Kit (Thermo Fisher Scientific, MA, USA) according to the manufacturer's recommendations. The isolated total RNA was quantified using a

spectrophotometer. Total RNA was converted to cDNA using TaqMan™ Advanced miRNA cDNA Synthesis Kit (Thermo Fisher Scientific, MA, USA). Quantitative real time-polymerase chain reaction (qRT-PCR) analysis was performed using Roche LightCycler® 96 System with TaqMan® MicroRNA Assay kit for hsa-miR-9-5p and endogenous control RNU48. The total reaction volume was 20 µl and contained the following components: 1:10 diluted miR-9 or RNU48 cDNA reaction product, 1 µl TaqMan® Advanced miRNA Assay (20×), 10 µl TaqMan® Fast Advanced Master Mix (2×), and 4 µl RNase free water (Thermo Fisher Scientific, MA, USA). qRT-PCR was then performed on the 96-well plate using the following protocol: 95 °C for 20 s, 40 cycles of 95 °C for 1 s, and 60 °C for 20 s. The relative miR9 level was normalized to the expression of the endogenous control RNU48 for each sample and calculated using the $2^{-\Delta\Delta Ct}$ method. The experiment was performed three times in triplicate.

MTT Assay

The cell viability post-OGD was measured using MTT assay. SH-SY5Y cells were seeded in transparent 96 multi-well plates at a density of 1×10^4 cells/well, and cell viability was measured 24 h following OGD using 3-(4,5-dimethylthiazol-2-yl)-2,5-diphenyltetrazolium bromide (MTT) (0.5 mg/ml) as previously described (Davis et al. 2018). The absorbance was measured at 570 nm using a microplate reader (TECAN, Infinite200 pro, Switzerland).

ATP Assay

SH-SY5Y cells were seeded in opaque white 96-well plates at a density of 1×10^4 cells/well for ATP assay. The CellTiter-Glo® 3D Cell Viability Assay (Promega, Madison, WI, USA) was used to determine the amount of ATP in the cells 24-h post-OGD/R according to the manufacturer's instructions. An equal volume of CellTiter-Glo® 3D Reagent was added corresponding to the volume of cell culture medium present in each well. The contents were mixed for 5 min to induce cell lysis. The plate was incubated at room temperature for an additional 25 min to stabilize the luminescent signal, and the luminescence was recorded using microplate reader (TECAN, Infinite200 pro, Switzerland) with an integration time of 1 s.

Docking and Molecular Dynamics (MD) Simulation

Structure-Based virtual screening of FDA drug database against HDAC4 was employed to identify a small molecule alternative to upregulate miR-9 and repurpose drugs for the treatment of ischemic stroke. The crystal structure of the protein, HDAC4 (PDB ID: 2VQM), was retrieved from Protein Data Bank (PDB) (http://www.rcsb.org/pdb/home/home.do). The zinc binding catalytic domain of HDAC4 was identified as the active site (Bottomley et al. 2008) to create a receptor grid for docking. The food and drug administration (FDA)-approved drug structures were obtained from DrugBank (http://www.drugbank.ca) (Wishart et al. 2008) to identify the ligand binding to HDAC4. The prepared ligands were docked to the generated receptor grid for the protein HDAC4 using structure-based virtual screening module of Schrodinger suite, and the parameters were set as already described (Davis et al. 2018). The molecular weight of ligands to be docked to HDAC4 was set to less than or equal to 600. The glide score was analyzed, and the best ligand conformation was selected.

MD simulation renders an account of protein–ligand motion in a simulated biological environment at an atomic level. The PRODRG server (http://davapc1.bioch.dundee.ac.uk/cgi-bin/prodrg) provided topologies and parameters for the ligand. A 20 ns MD simulation of the selected protein–ligand complex was executed using Gromacs v5.1.1 software with Gromos53a6 force field as already described (Fayaz and Rajanikant 2014).

Drug Affinity Responsive Target Stability (DARTS) Assay

The virtually predicted glucosamine–HDAC4 interaction was verified using DARTS assay as previously described (Davis et al. 2018; Pai et al. 2015). Briefly, the protein was isolated using M-per Mammalian Protein Extraction Reagent (Thermo Fisher Scientific, MA, USA) and centrifuged at 18,000 × g at 4 °C for 10 min. The protein concentration was measured using Pierce BCA protein assay kit (Thermo Fisher Scientific, MA, USA). The protein (500 µg/ml) isolated from SH-SY5Y cells was treated with 300 µM of glucosamine (Sigma-Aldrich, MO, USA) for 45 min at 37 °C and then treated with pronase (0.5 and 0.2 µg/ml) (Roche Holding AG, Basel, Switzerland) for 30 min at 37 °C. The pronase digestion was ceased by adding SDS–PAGE sample loading buffer and heated at 95 °C for 5 min. The protein samples were run on a 10% Bis-Tris gel and stained using Coomassie blue. The protected protein bands were further analyzed by matrix-assisted laser desorption/ionization time-of-flight mass spectrometry (MALDI-TOF MS). The experimental data containing the peptide mass (m/z) values were analyzed using MASCOT peptide mass fingerprint.

Post-OGD Glucosamine Treatment and Cell Viability Measurement

Post-ischemic neuroprotective efficacy of glucosamine was evaluated in SH-SY5Y cells subjected to 2 h of OGD as described earlier. Cells were treated with 0, 0.1, 0.5, 1, or

5 μM of glucosamine 1 h after the completion of OGD. The control cells remained untreated and were kept under a normoxic condition with 5% CO_2 and 95% air in DMEM/F12 containing 10% FBS.

Lactate Dehydrogenase (LDH) Assay

Cell death was measured 24-h post-OGD using Pierce™ LDH Cytotoxicity Assay Kit (Thermo Fisher Scientific, MA, USA) according to the manufacturer's protocol. The absorbance was measured at 490 nm and 680 nm (reference) using microplate reader (TECAN, Infinite200 pro, Switzerland). LDH in the withdrawn culture medium was quantified, and the results were expressed as a percentage of cell viability.

Annexin V/Propidium Iodide (PI) Quantification

Cell death was assessed using Dead cell apoptosis kit Annexin V/PI (Thermo Fisher Scientific, MA, USA). SH-SY5Y cells were seeded in opaque black 96-well plates at a density of 1×10^4 cells/well. The assay was performed according to the manufacturer's guidelines, and the fluorescence intensity was measured using microplate reader (TECAN, Infinite200 pro, Switzerland) at fluorescence emission of 530 nm and 575 nm.

5-Bromo-2′-Deoxyuridine (BrdU) Assay

To analyze cell proliferation, 5-Bromo-2′-deoxyuridine Labeling and Detection Kit I (Sigma-Aldrich, MO, USA) was used 24-h post-OGD according to the manufacturer's protocol. SH-SY5Y cells were grown on matrigel coated coverslips in 24-well plates at a density of 0.5×10^5 cells/well. After labeling the cells with BrdU, the coverslips were mounted onto the glass slides using SlowFade™ Diamond Antifade Mountant with DAPI (Thermo Fisher Scientific, MA, USA). The number of BrdU-positive cells and total DAPI nuclei was counted under a 20x objective (Nikon Eclipse Ti, Nikon Instruments, Tokyo, Japan), and the percentage of BrdU/DAPI was determined.

Neurite Outgrowth Assay

SH-SY5Y cells were seeded on matrigel coated cover slips in 24-well plates with an initial density of 0.5×10^5 cells/well. After 24 h and 48 h of OGD/R, neurite outgrowth was measured using Neurite Outgrowth Staining Kit (Thermo Fisher Scientific, MA, USA) according to the manufacturer's guidelines. The cells were mounted on glass slides using SlowFade™ Diamond Antifade Mountant with DAPI (Thermo Fisher Scientific, MA, USA) and visualized under a fluorescent microscope (40×) (Nikon Eclipse Ti, Nikon Instruments, Tokyo, Japan). Simple Neurite Tracer, an ImageJ plugin, was used to trace the neurites and the neurite length was measured.

Total RNA Isolation, cDNA Conversion, and qRT-PCR Analysis

Total RNA was extracted from the harvested cells using RNAqueous™-Micro Total RNA Isolation Kit (Thermo Fisher Scientific, MA, USA) according to the manufacturer's recommendations and quantified using a spectrophotometer. cDNA was synthesized from the isolated total RNA using Verso cDNA synthesis kit (Thermo Fisher Scientific, MA, USA) as instructed in the manual. Reverse transcription was performed at 42 °C for 30 min, 95 °C for 5 min followed by 4 °C hold. The converted cDNA was subjected to qRT-PCR using the following primers (Eurogentec, Liège, Belgium) to determine the expression level of the genes: BCL2, VEGF, NFκB1, TNF-α, IL1-β, and iNOS.

GAPDH	Forward primers: TCATGGTAT GAGAGCTGGGGA Reverse primers: AGTGATGGC ATGGACTGTGG
VEGF	Forward primer: GCCTTTTTG CAGTCCCTGTG Reverse primer: AGGCAGGCA GCTAGAAACTG
NFκB1	Forward primer: TTCCCGATC TGAGTCCAGGT Reverse primer: GCTTGTCTC GGGTTTCTGGA
BCL2	Forward primer: TGAAACTCC CTTAGCCCTGC Reverse primer: CAGGGCGTA TCAAGGGAGAG
iNOS	Forward primer: TATGAACGC CAGCATGAGCC Reverse primer: CACCCCTGT TTCAACGACCT
IL-1β gene	Forward primer: GTCTCAGCG TCTCCACTGAC Reverse primer: TCACACATG AACGTAGCCGT
TNF-α	Forward primer: TCTGGCACA CAGAAGACACT Reverse primer: GGCCAGAGG GCTGATTAGAG

qRT-PCR analyses were performed using DyNAmo™ ColorFlash SYBR Green qPCR Kit (Thermo Fisher Scientific, MA, USA) on Roche Lightcycler 96 system (Roche Holding AG, Basel, Switzerland) according to the provided guidelines. Glyceraldehyde 3-phosphate dehydrogenase (GAPDH) served as the internal control, and relative gene expression was evaluated using $2^{-\Delta\Delta CT}$ method.

Statistical Analysis

The data were analyzed with GraphPad Prism version 5 for Windows (GraphPad software, San Diego, CA, USA) and are expressed as mean ± standard error of the mean (SEM) in graphics and text representations. One-way analysis of variance (ANOVA) followed by Bonferroni's multiple comparison test was utilized to obtain the difference between three or more groups. Student's *t* test was performed to analyze two independent groups. A *p* value of less than 0.05 was considered statistically significant. Each experiment was performed thrice in triplicate.

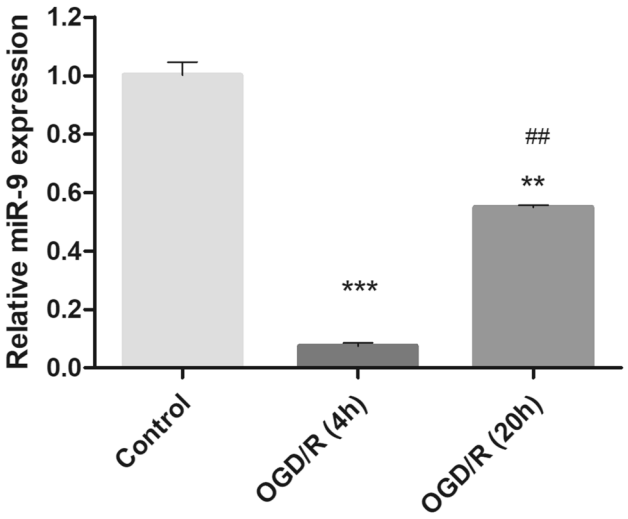

Fig. 1 miR-9 expression analysis in SH-SY5Y cells subjected to OGD after 4-h and 20-h reoxygenation. The relative expression of miR-9 was normalized to RNU48. Data are represented as mean ± SEM, where $^{***}p < 0.001$, $^{**}p < 0.01$ versus control, $^{\#\#}p < 0.01$ versus OGD/R (4 h) denoted significance. OGD/R represents oxygen-glucose deprivation/reoxygenation

Results

Reduced miR-9 Expression Following OGD

Oxygen-glucose deprivation significantly reduced miR-9 expression following 4-h ($^{***}p < 0.001$ vs control) and 20-h ($^{**}p < 0.01$ vs control) reoxygenation when compared with the control group (Fig. 1). However, there was a marginal increase in endogenous miR-9 expression at 20-h post-OGD [$^{\#\#}p < 0.01$ vs OGD/R(4 h)].

miR-9 Upregulation Promotes Neuronal Survival In Vitro

To examine the effect of miR-9 in neuronal cell viability following OGD, SH-SY5Y cells were transfected with miR-9 mimic, inhibitor, and the corresponding miRNA negative controls for 10 h before OGD (Fig. 2a). The transfection efficiency of miR-9 was evaluated 24 h after OGD using qRT-PCR (Supplemental Fig. 1). Subsequently, the cells were tested for viability at 24-h post-OGD using MTT assay. The average cell viability was significantly reduced (61.9%) in the vehicle group exposed to OGD/R when compared with the control group kept under normoxia (100%) ($^{***}p < 0.001$ vs control). The cells transfected with miR-9 mimic and subjected to OGD/R showed a significant increase in average cell viability (82.89%; $^{\#\#}p < 0.01$ vs vehicle). However, the miR-9 antagomir and the miRNA negative control-transfected cells did not exhibit any significant change. The cell viability comparison with miRNA negative controls

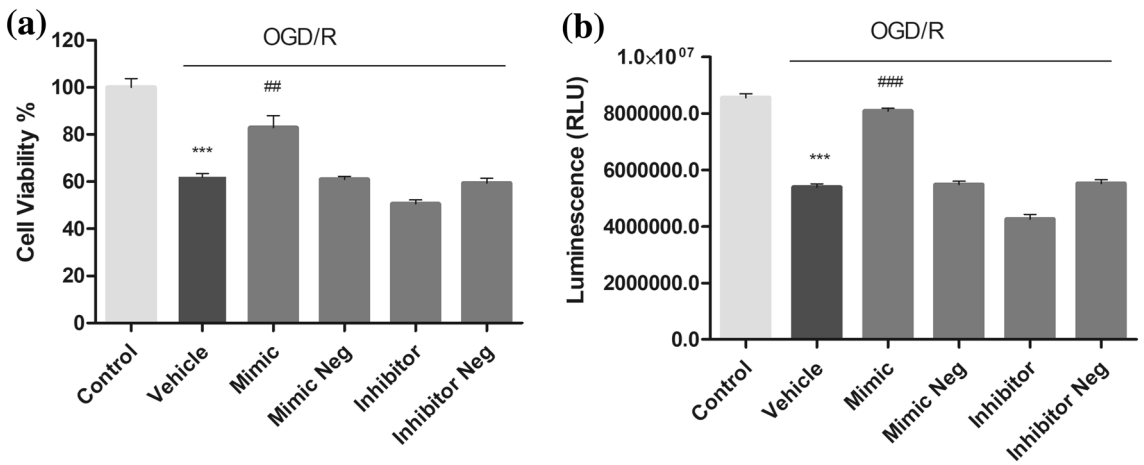

Fig. 2 miR-9 transfection and cell viability measurement **a** The graph shows the post-OGD percentage of cell viability (**b**) and level of ATP in terms of relative luminescence unit (RLU), in miR-9 mimic, inhibitor, and the corresponding negative control-transfected cells. Data are represented as mean ± SEM, where $^{***}p < 0.001$ versus control, $^{\#\#\#}p < 0.001$, $^{\#\#}p < 0.01$ versus vehicle were considered significant

indicated the explicit neuroprotective role of miR-9 mimic following OGD.

In addition, the effect of miR-9 on cellular ATP was measured to determine the metabolic activity of cells. ATP is a marker for cell viability present in all metabolically active cells. ATP can induce cell proliferation and differentiation arbitrating different pathophysiological functions based on the target cell. The ATP levels were quantified in terms of luminescence and miR-9 mimic-transfected cells displayed a significant increase in ATP, in contrast to OGD/R exposed cells that caused a reduction in the intracellular ATP (***$p < 0.001$ vs control, ###$p < 0.001$ vs vehicle) (Fig. 2b). Hence, miR-9 upregulation directly enhanced ATP levels in cells exposed to OGD/R and further established its function in neuronal survival.

Glucosamine Formed Docked Complex with HDAC4

miR-9 forms a positive feedback loop with HDAC4 to stabilize its expression (Davila et al. 2014). Besides, miR-9 and HDAC4 were predicted to be the significant regulators of post-stroke-induced neurogenesis (Nampoothiri et al. 2018). Therefore, in this study, we employed a drug repositioning strategy to amplify miR-9 expression through the structure-based screening of FDA-approved drugs that target HDAC4. Small-molecule-mediated regulation of miRNAs is of great therapeutic significance and could act as an attractive alternative to using exogenous miRNAs (Lee et al. 2018). Docking-based virtual screening of FDA-approved drug database identified Glucosamine, S-Adenosylmethionine, Amoxicillin, Dasatinib, and Plerixafor as the potential inhibitors of HDAC4. Glucosamine emerged as the top hit with the best docking score of −8.73 (Table 1). The plausible binding mode of glucosamine to the active site of HDAC4 is depicted in Fig. 3 a, b.

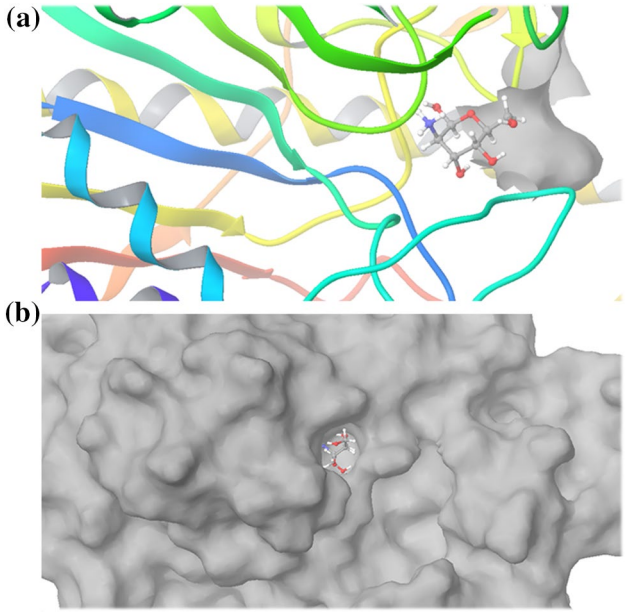

Fig. 3 Illustration of glucosamine docked to the active site of HDAC4 **a** Ribbon representation of docked complex of HDAC4 and glucosamine (ball and stick chemical structure) **b** The 3D molecular surface representation of HDAC4 docked to glucosamine

MD Simulation Confirmed the Interaction of Glucosamine with HDAC4

MD simulation is construed as a computational microscope that uncovers the interaction between atoms in a biomolecule with another small molecule at spatial and temporal scales. It enables the computation of positions, energies, and velocities during the interaction, which is otherwise challenging to deduce experimentally (Dror et al. 2012). Molecular docking provided a virtual representation of glucosamine-HDAC4 interaction, and MD simulation extrapolated the stability of glucosamine-HDAC4 complex by considering solvent effect and protein flexibility in a simulated biological environment. The root-mean-square deviation (RMSD) value provided the measure of the dynamic stability of the MD trajectories. RMSD plot showed that the interaction between glucosamine and HDAC4 was stable during the course of simulation. The RMSD of Glucosamine in the docked complex was stable at 0.5 nm (Fig. 4a). The number of H-bonds formed between the ligand glucosamine and the protein receptor HDAC4 during 20 ns of simulation is depicted graphically (Fig. 4b).

Table 1 Top five FDA-approved drugs targeting HDAC4 obtained from molecular docking analysis

Generic drug name	Molecular formula	Molecular weight	Docking score
Glucosamine	C6H13NO5	179.1711	−8.729463
S-Adenosylmethionine	C15H23N6O5S	399.445	−8.377353
Amoxicillin	C16H19N3O5S	365.404	−8.002663
Dasatinib	C22H26ClN7O2S	488.006	−7.794825
Plerixafor	C28H54N8	502.782	−7.717125

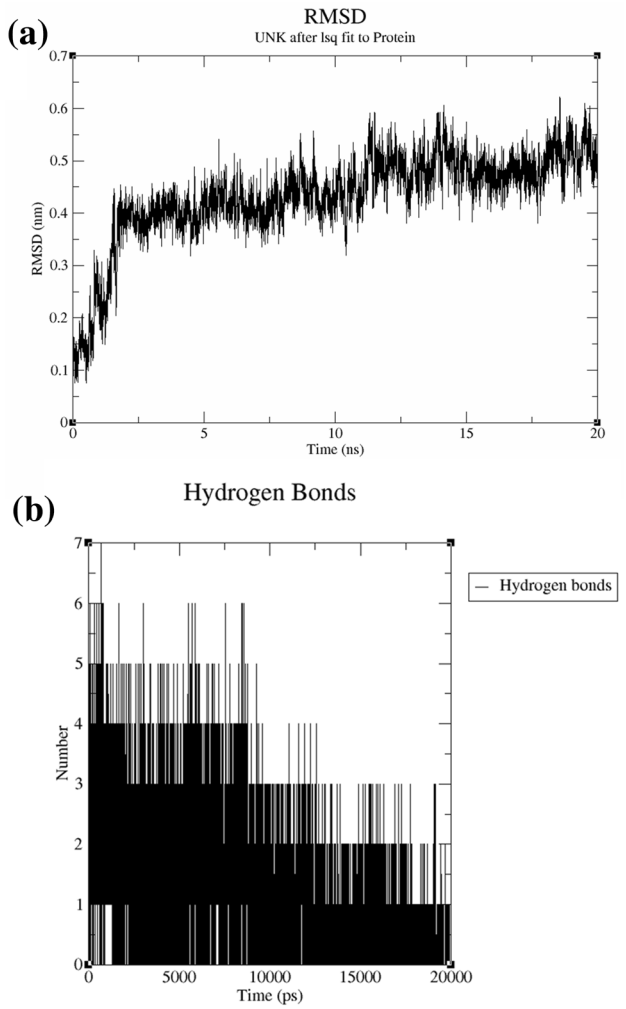

Fig. 4 **a** RMSD plots of protein–ligand complexes. RMSD of glucosamine compared to the initial position in complex with HDAC4 along 20 ns of MD simulation. **b** Calculation of number of H-bonds. Number of H-bonds formed between Glucosamine and HDAC4 during 20 ns of MD simulation

DARTS Assay Validated the Glucosamine–HDAC4 Interaction

The affinity of glucosamine–HDAC4 interaction was determined using DARTS assay. The assay is based on the reduced susceptibility of the target protein to protease-induced degradation as the protein stabilizes following small-molecule treatment (Pai et al. 2015). The glucosamine-treated cell lysate was partially digested with pronase to identify the proteins bound to glucosamine. The proteins were separated by SDS–PAGE and it was observed that the glucosamine-treated sample protected the band corresponding to 140 kDa representing HDAC4 protein (Fig. 5a). There was no band in the pronase-digested sample without glucosamine. The protected band was verified to be HDAC4 by MALDI-TOF MS. The peak corresponding to HDAC4 has been marked in the mass spectrogram (Fig. 5b).

Glucosamine Treatment Promoted Neuronal Survival Post-OGD

One-hour post-OGD treatment of cells with 0.5 µM of glucosamine rendered the highest average cell viability of 88.19% ($^{\#\#\#}p < 0.001$ vs vehicle) against vehicle-treated cells exposed to OGD/R (63.18%; $^{***}p < 0.001$ vs control) (Fig. 6a). LDH assay also substantiated that glucosamine-treated cells (0.5 µM) significantly improved cell viability ($^{\#\#\#}p < 0.001$ vs vehicle) (Fig. 6b). Thus, the glucosamine concentration of 0.5 µM was chosen for the subsequent studies carried out in SH-SY5Y cells.

Glucosamine Treatment Upregulated miR-9 Post-OGD

miR-9 expression was quantified in glucosamine-treated SH-SY5Y cells after 4 h and 20 h of OGD. At 4-h post-OGD, glucosamine-treated cells showed a slight increase in miR-9 expression [$^{\#}p < 0.05$ vs vehicle-treated cells exposed to OGD/R (4 h)] (Fig. 7a). Interestingly, glucosamine exhibited a significant increase in miR-9 expression at 20 h following OGD [0.8125-fold, $^{\#\#\#}p < 0.001$ vs vehicle-treated cells exposed to OGD/R (20 h)] (Fig. 7b). These results corroborated that glucosamine could modulate miR-9 expression by targeting HDAC4 and could be possibly used as an alternative to exogenous miR-9 mimic to upregulate miR-9. We further compared the effect of miR-9 mimic and glucosamine administration on neuronal death, neuronal proliferation, neurite outgrowth, and mRNA expression of BCL2, NFκB1, and VEGF.

miR-9 Mimic and Glucosamine Alleviated Neuronal Apoptosis and Necrosis

To evaluate the effect of miR-9 upregulation and glucosamine treatment on neuronal death, we quantified the fluorescence intensity of PI- and Annexin V-stained SH-SY5Y cells. At 530 nm and 575 nm, glucosamine-treated and miR-9-upregulated cells emitted significantly low fluorescence as opposed to the vehicle-treated OGD/R-induced cells ($^{\#\#\#}p < 0.001$ vs vehicle). This observation showed that glucosamine and miR-9 mimic alleviate neuronal apoptosis and necrosis.

Post-OGD BrdU Incorporation in miR-9-Transfected and Glucosamine-Treated Cells

The effect of miR-9 upregulation and glucosamine on cellular proliferation following OGD/R was further evaluated

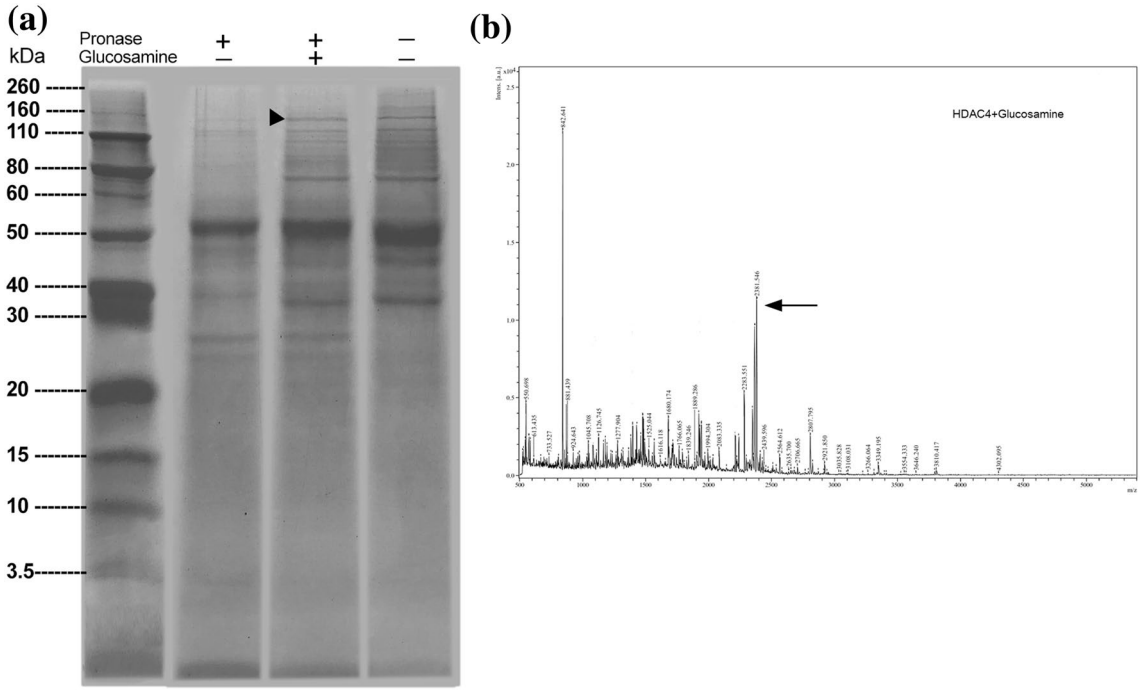

Fig. 5 Experimental validation of glucosamine binding to HDAC4 **a** Protein separation using DARTS assay, where black arrowhead indicates the protected band corresponding to HDAC4 in glucosamine-treated sample with optimum pronase digestion **b** Mass spectrogram confirmed the binding of HDAC4 with glucosamine

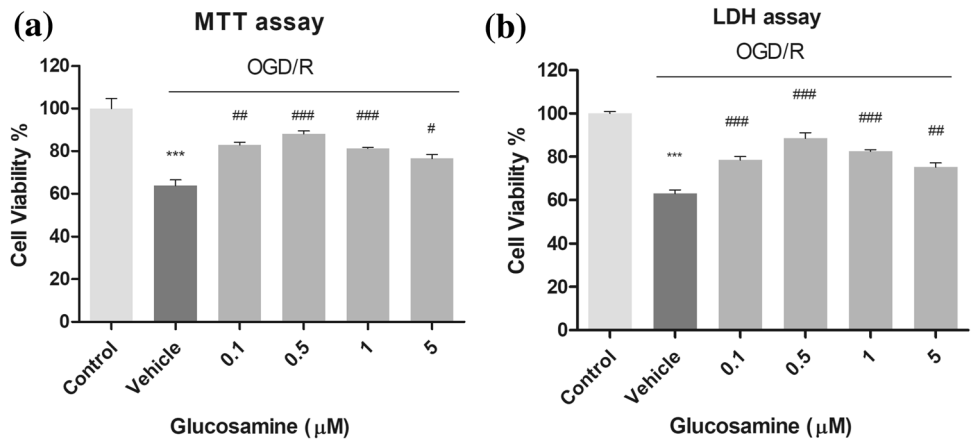

Fig. 6 Post-ischemic neuroprotection conferred by glucosamine in SH-SY5Y cells (**a**) Post-OGD percentage cell viability in cells treated with different concentration of glucosamine (0.1, 0.5, 1, or 5 μM) obtained using **a** MTT assay **b** LDH assay. The cells exposed to OGD/R and treated with PBS represent the vehicle group. Data are represented as mean ± SEM, where $^{***}p < 0.001$ versus control, $^{\#}p < 0.05$, $^{\#\#}p < 0.01$, $^{\#\#\#}p < 0.001$ versus vehicle were considered significant

by labeling SH-SY5Y cells with BrdU (Fig. 9a). The cell proliferation reduced by 20.5% in vehicle-treated cells exposed to OGD/R compared with the control ($^{**}p < 0.01$ vs control). At 24-h post-OGD, miR-9 upregulation significantly increased the BrdU-stained cells by 21.15% compared to the vehicle-treated OGD-induced cells ($^{\#}p < 0.05$ vs vehicle), whereas miR-9 inhibition did not have any significant effect on cellular proliferation ($p > 0.05$). Glucosamine treatment remarkably enhanced cell proliferation after 24 h of OGD/R with a 33.2% increase in BrdU-positive cells ($^{\#\#\#}p < 0.001$ vs vehicle) (Fig. 9b). These results suggest the positive effect of miR-9 upregulation and glucosamine treatment in promoting cellular proliferation after ischemic stroke in vitro.

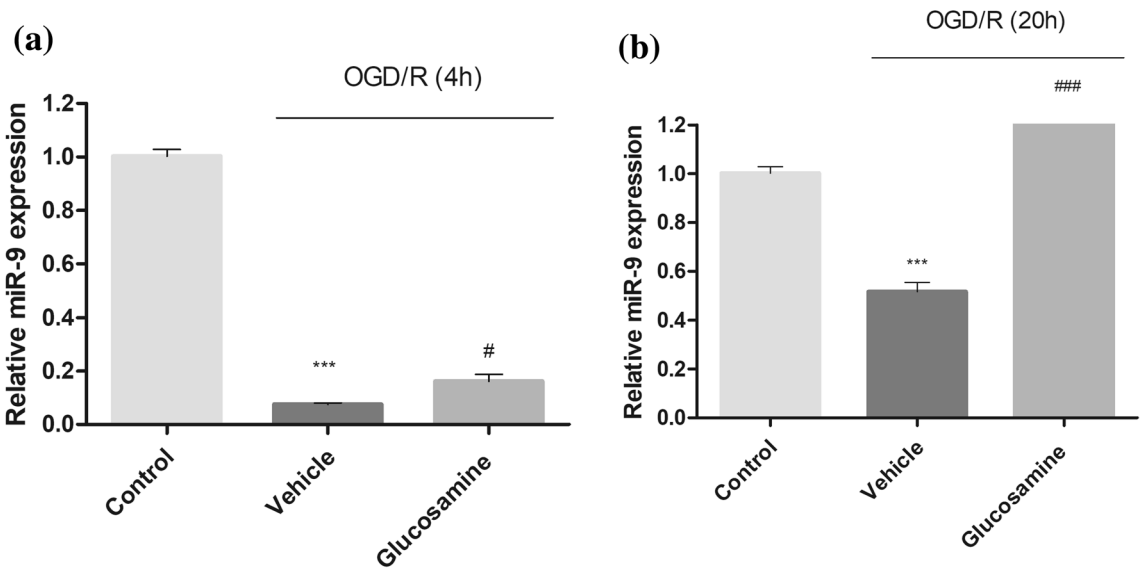

Fig. 7 Glucosamine treatment upregulated miR-9 expression **a** 4-h post-OGD **b** 20-h post-OGD. Data are represented as the mean of fold change and error bars depict SEM. The values with $^{***}p < 0.001$ versus control, $^{\#}p < 0.05$, $^{\#\#\#}p < 0.001$ versus vehicle were considered significant

Effect of miR-9 Mimic and Glucosamine on Neurite Outgrowth Post-OGD

To assess the role of miR-9 in neurite outgrowth, SH-SY5Y cells were transfected with miR-9 mimic, antagomir, and corresponding negative controls prior to OGD exposure (Figs. 10, 11). At 24-h post-OGD, the vehicle-treated cells subjected to OGD showed stubby neurite outgrowth with 2.79 cm average neurite length ($^{***}p < 0.001$ vs control) while those transfected with miR-9 mimic exhibited a greater neurite length of 4.93 cm ($^{\#\#\#}p < 0.001$ vs vehicle) (Fig. 12a). The average neurite length further increased to 8.68 cm at 48 h following OGD/R in miR-9 mimic-transfected cells ($^{***}p < 0.001$ vs control, $^{\#\#\#}p < 0.001$ vs vehicle), whereas miR-9 antagomir inhibited neurite outgrowth ($^{***}p < 0.001$ vs control, $^{\#}p < 0.05$ vs vehicle) (Fig. 12b). Further, we detected that glucosamine-treated cells promoted neurite outgrowth after OGD. The neurite outgrowth was measured at 24-h and 48-h post-OGD with an average neurite length of 4.8 cm ($^{\#\#\#}p < 0.001$ vs vehicle) and 7.56 cm ($^{**}p < 0.01$ vs control, $^{\#\#\#}p < 0.001$ vs vehicle), respectively (Fig. 12 a,b).

Co-overexpression of VEGF and BCL2 Inhibits Ischemic Apoptosis

OGD/R resulted in a significant reduction in BCL2 expression (0.379-fold decrease; $^{**}p < 0.001$ vs control), whereas BCL2 expression was increased by 1.23-fold in miR-9 mimic-transfected ($^{\#\#\#}p < 0.001$ vs vehicle) and 1.07-fold in glucosamine administered cells ($^{\#\#\#}p < 0.001$ vs vehicle). It was noted that miR-9 upregulation raised BCL2 levels 0.692-fold greater than the control group ($^{***}p < 0.001$ vs control). However, miR-9 inhibition further attenuated BCL2 gene expression in comparison with the control as well as OGD/R group ($^{***}p < 0.001$ vs control, $^{\#}p < 0.05$ vs vehicle) (Fig. 13a).

We quantified VEGF expression in miR-9 mimic and glucosamine-treated cells following OGD/R. VEGF expression significantly decreased in OGD group treated with vehicle ($^{***}p < 0.001$ vs control), whereas miR-9 mimic and glucosamine treatment elevated VEGF levels post-OGD ($^{\#}p < 0.05$ vs vehicle). miR-9 inhibition reduced the VEGF expression as opposed to the control as well as OGD group ($^{**}p < 0.01$ vs control, $^{\#}p < 0.05$ vs vehicle) (Fig. 13b).

miR-9 Mimic and Glucosamine Reduced the Expression of Pro-inflammatory Genes

The mRNA expression of pro-inflammatory genes such as NFκB1, TNF-α, IL-1β, and iNOS was quantified. NFκB1 mRNA level increased by 2.27-fold in cells subjected to ischemia ($^{***}p < 0.001$ vs control), which was found to subside with miR-9 upregulation (2.01-fold decrease; $^{\#\#\#}p < 0.001$ vs vehicle) and glucosamine treatment (2.16-fold decrease; $^{\#\#\#}p < 0.001$ vs vehicle). In contrast, miR-9 antagomir elevated NFκB1 gene expression and was statistically significant compared with the control cells (2.11-fold increase; $^{***}p < 0.001$ vs control) (Fig. 13c). Further, the levels of TNF-α (2.14-fold, $^{***}p < 0.001$), IL-1β (6.22-fold, $^{***}p < 0.001$), and iNOS (0.585-fold, $^{***}p < 0.001$) increased following OGD/R compared with the control group. It was also observed that, miR-9 mimic as well

glucosamine treatment significantly decreased the expression of pro-inflammatory genes, TNF-α and IL-1β and iNOS ($^{###}p < 0.001$ vs vehicle) (Fig. 13 d–f).

Discussion

The present study was conceptualized to investigate the role of miR-9 upregulation in neuronal proliferation and regeneration in response to OGD injury *in vitro*. Ischemic stroke disrupts the structural and functional integrity of brain offering multiple challenges in the development of an efficient neurotherapy. Only a multifaceted therapeutic approach that promotes neuronal repair, as well as survival, can facilitate long-term functional recovery against ischemic stroke. To accomplish this, it is essential to determine the critical miRNAs, the post-transcriptional and the translational regulators, that coordinate neuropathological and neurodevelopmental processes.

In view of increasing pertinence of miRNAs in ischemic stroke, we computationally predicted that miR-9 and HDAC4 significantly modulate post-stroke-induced neurogenesis (Nampoothiri et al. 2018). miR-9 is evolutionarily conserved and abundantly expressed in the neurogenic regions of the brain with implications in the embryonic and adult neural progenitor differentiation (Coolen et al. 2013). A few recent reports have delved into the role of miR-9 in alleviating neuronal apoptosis following ischemic stroke (Wei et al. 2016; Chen et al. 2017). However, there is no experimental evidence signifying the vital role of miR-9 in post-ischemic neuronal regeneration.

The prime rationale of this study was to explore whether miR-9 upregulation vanguards post-ischemic neuronal regeneration and survival. We quantitatively assessed the expression of miR-9 in SH-SY5Y cells at 4 h and 20 h following OGD, where the miR-9 level significantly reduced at both the time points (Fig. 1). The slight increase in miR-9 expression at 20-h post-OGD could be ascribed to the initiation of endogenous neuronal restoration during 20-h reoxygenation after the cells were exposed to OGD. Furthermore, miR-9 mimic transfection increased the cell viability to 82.89% against 61.9% in vehicle-treated OGD/R-induced cells (Fig. 2a). A previous study indicated that miR-9 level decreases in an in-vitro and in-vivo model of ischemic stroke, while miR-9 upregulation impedes neuronal apoptosis by targeting the pro-apoptotic gene, BCL2L11 (Wei et al. 2016). Another report indicated the association of long noncoding TUG1 with reduced miR-9 and increased BCL2L11 expression following ischemic stroke (Chen et al. 2017). To the contrary, a recent study suggested that miR-9 upregulation contributes to dementia following chronic cerebral hypoperfusion in rats. The authors implied that miR-9 inhibition results in an increased BACE1 and reduced CREB1 expression restoring the learning and memory impairment (Xie et al. 2017). However, the study contradicts the function of BACE1 in neuropathological abnormalities and cognitive deficits. Many reports support the association of upregulated BACE1 with hypoxia, ischemic injury, and Alzheimer's disease (Chami and Checler 2012; Guglielmotto et al. 2009; Laird et al. 2005). Moreover, the increase in miR-9 expression during chronic brain injury might be associated with the initiation of endogenous brain repair mechanisms.

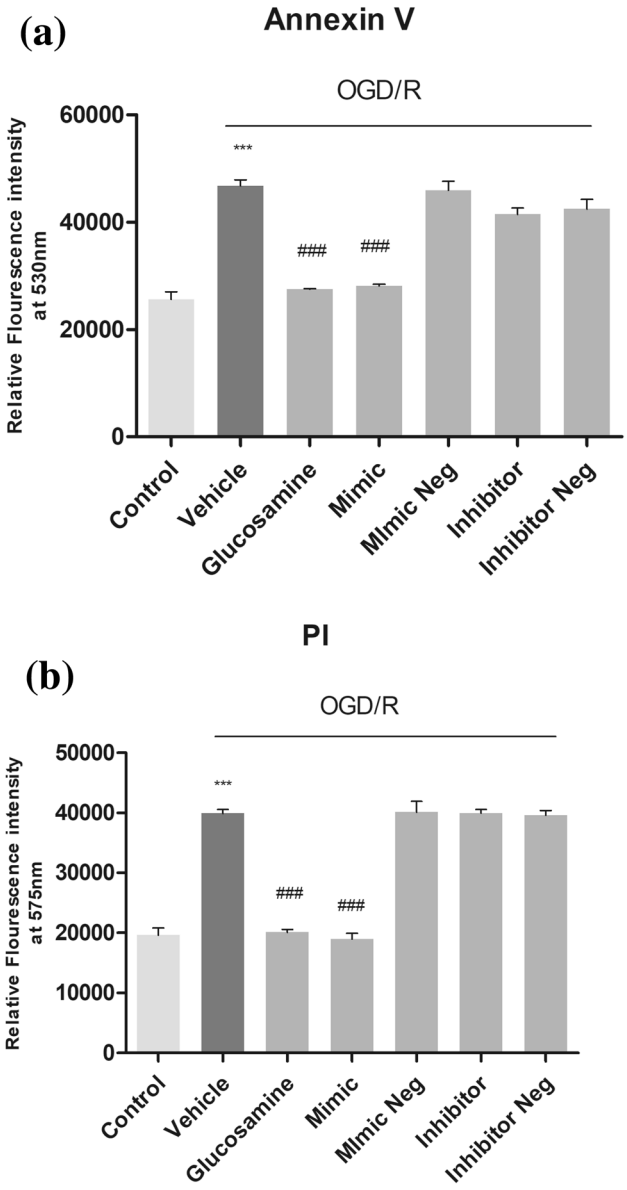

Fig. 8 Annexin V/PI assay. The cell death was evaluated by quantifying the fluorescence intensity of Annexin V- and PI-stained SH-SY5Y cells following OGD/R at **a** 530 nm, and **b** 575 nm, respectively. Data are represented as mean ± SEM, where $^{***}p < 0.001$ versus control, $^{\#}p < 0.05$, $^{###}p < 0.001$ versus vehicle were significant

We further employed a structure-based screening approach to identify a suitable pharmacological intervention that targeted HDAC4 and facilitated the consequent elevation of miR-9 expression. Ischemic stroke disrupts the acetylation of histones H3 and H4 with the increased activity of HDACs (Langley et al. 2009). Non-selective HDAC inhibitors, such as, valproic acid and trichostatin have been reported to confer neuroprotection in animal models of ischemic stroke (Ziemka-Nalecz and Zalewska 2014). Besides, there has been a concerted effort to identify class-specific HDAC inhibitors as the post-ischemic mechanistic action of each HDAC is different. HDAC4, a class IIa-specific HDAC, has been reported to shuttle between nucleus and cytoplasm during ischemic stroke (Bolger and Yao 2005). Under ischemic stress, HDAC4 translocates to nucleus from cytoplasm, and nuclear accumulation of HDAC4 mediates neuronal death (Yuan et al. 2016). Also, it has been reported that miR-9 negatively regulates HDAC4 and reducing HDAC4 level raises miR-9 expression. This mechanism was reported to promote the neurogenic capacity of neural precursor cells (Davila et al. 2014). Hence, we further postulated that the identification of a small molecule binding to HDAC4 might aid in the regulation of miR-9 expression post-ischemia.

Drug repositioning has become one of the most sought-after therapeutic strategies enabling the testing of generic drugs at the pre-clinical and clinical levels (Ashburn and Thor 2004). This approach reduces the cost and time of drug development as the physicochemical and pharmacological properties of these drugs are previously known (Ashburn and Thor 2004). In this study, 1425 FDA-approved drugs were virtually screened for their ability to bind to HDAC4 and glucosamine emerged as the top hit (Fig. 3). MD simulation supported the molecular docking result (Fig. 4), which was further corroborated using DARTS assay/MALDI-TOF MS (Fig. 5).

This is the first known study providing a mechanistic insight into the positive effect of glucosamine on HDAC4

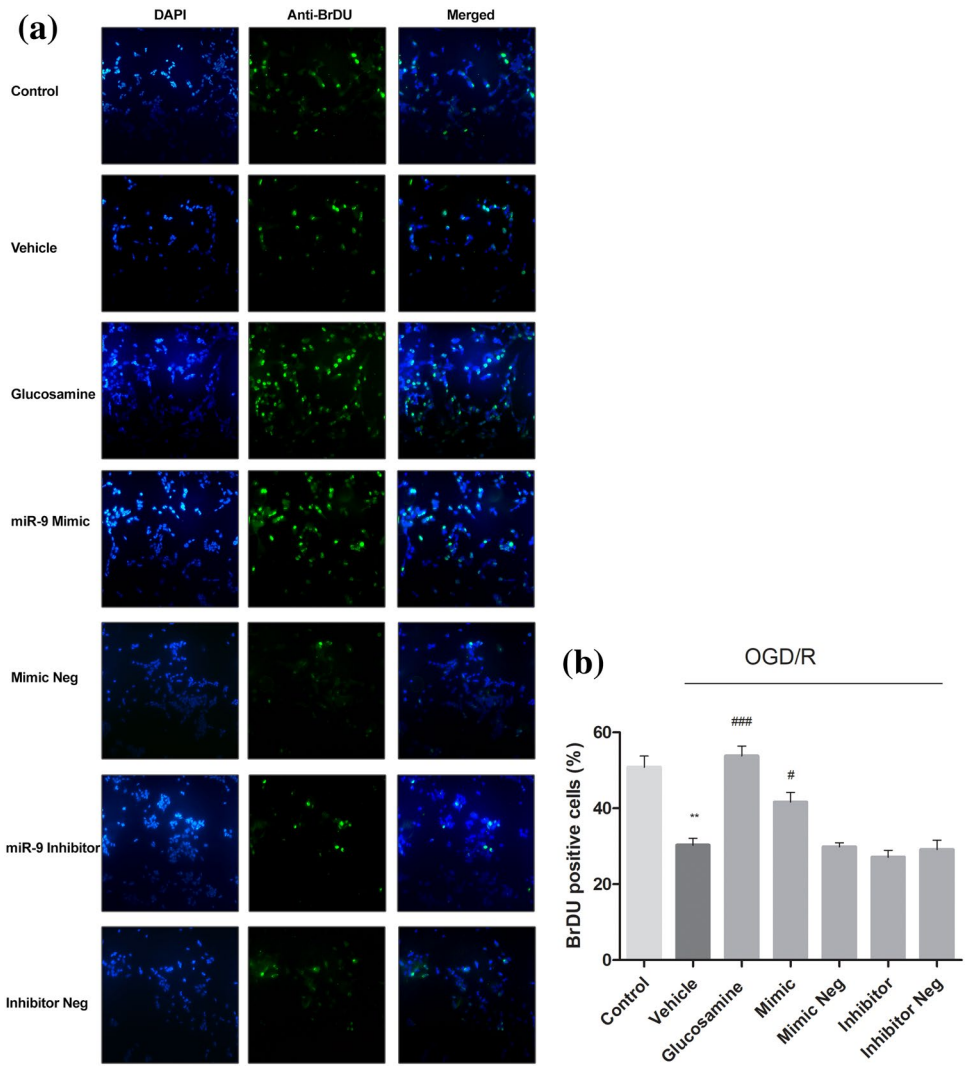

Fig. 9 BrdU incorporation in miR-9-transfected and glucosamine-treated cells following OGD/R. **a** The fluorescent images of miR-9/glucosamine-treated SH-SY5Y cells stained with BrdU (green) and DAPI (blue) following OGD/R (20×). A representative field for each experimental condition is shown. **b** The graph shows the average of BrdU-positive stained cells (%). The error bar indicates SEM and $^{**}p < 0.01$ versus control, $^{###}p < 0.001$, $^{#}p < 0.05$ versus vehicle were significant

serving as a premise to evaluate its role in miR-9 regulation. Glucosamine occurs naturally and is ubiquitously synthesized from glucose in all cells to form glycoprotein precursors such as UDP-N-acetyl-GlcN and UDPN-acetyl-galactosamine (Hawkins et al. 1997; Traxinger and Marshall 1991). A previous report revealed the post-ischemic neuroprotective efficacy of glucosamine through the suppression of microglial activation (Hwang et al. 2010). We showed that glucosamine increased cell viability post-OGD at a concentration as low as 0.5 μM (Fig. 6), thereby confirming its role in neuroprotection.

The next key objective of our study was to identify the effect of glucosamine treatment on miR-9 expression (Fig. 7). Though exogenous administration of miRNAs has yielded promising results, the challenges such as low transfection efficiency, low cellular uptake, serum instability, and high costs, still need to be addressed (Pecot et al. 2011). Small-molecule-mediated regulation of miRNAs would address these critical issues making ischemic stroke

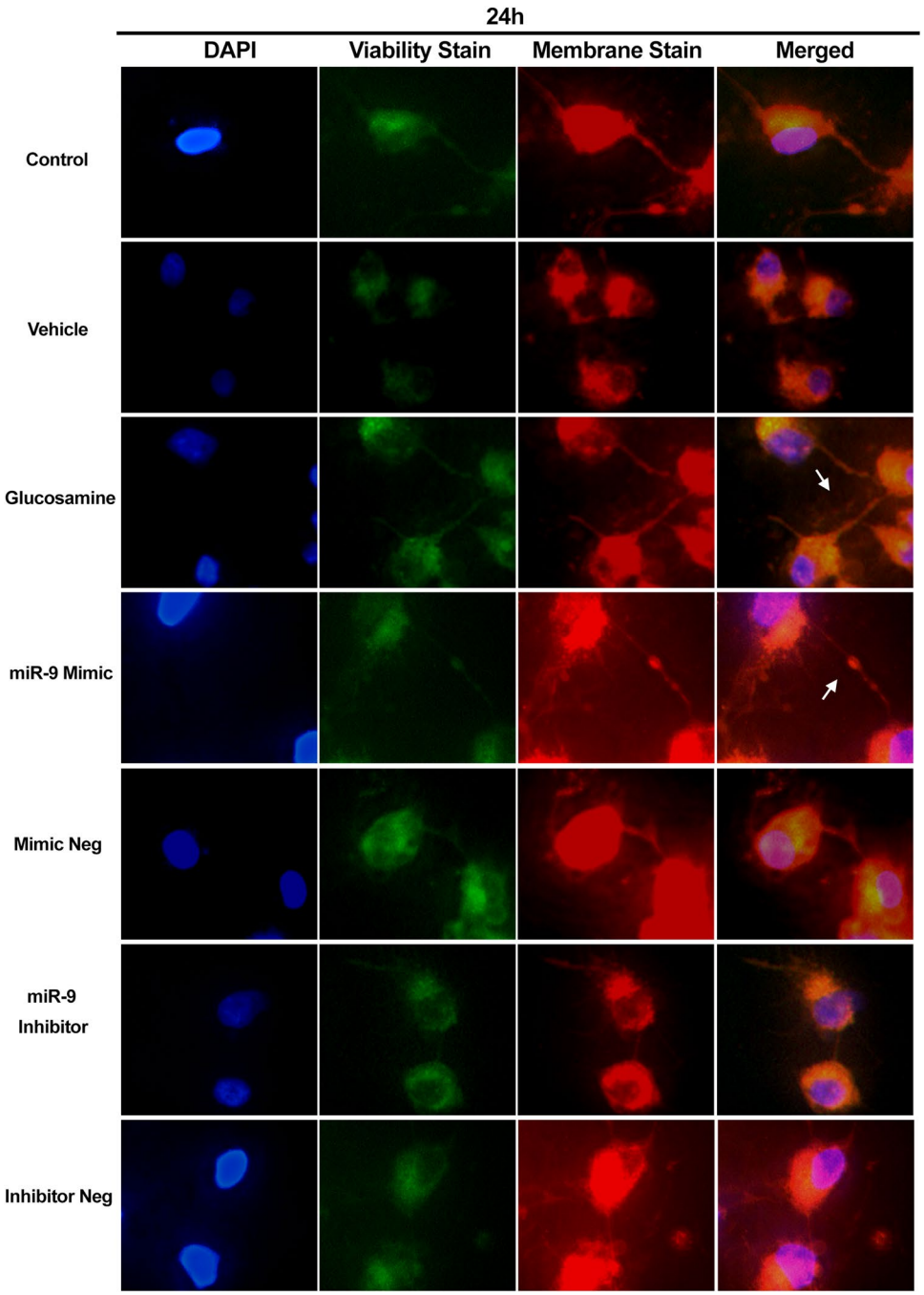

Fig. 10 Neurite outgrowth 24-h post-OGD/R. The fluorescent images demonstrate neurite outgrowth in miR-9/glucosamine-treated cells exposed to OGD after 24 h of reoxygenation (40 ×). The cells are stained with DAPI (blue), viability stain (green), and cell membrane stain (red)

therapeutics practically viable. Only a few studies have hitherto employed the small-molecule-mediated regulation of miRNAs (Young et al. 2010; Gumireddy et al. 2008; Xiao et al. 2014). Recently, miR-182 was upregulated using a small molecule to preclude ischemic-reperfusion-induced cardiac cell death (Lee et al. 2018). In our study, it was intriguing that glucosamine significantly elevated miR-9 expression post-OGD making it a suitable small molecule alternative for the upregulation of miR-9.

We further focussed on comparing the effect of glucosamine treatment and miR-9 mimic transfection in SH-SY5Y cells post-OGD. The reduced fluorescence emission in glucosamine-treated OGD-induced cells stained with Annexin V/PI supported the efficacy of miR-9 upregulation in alleviating neuronal necroptotic cell death (Fig. 8). miR-9 overexpression has been previously associated with the reduced neuronal apoptosis (Wei et al. 2016), and it could be deduced that miR-9 upregulation might also assuage necrotic cell death. Moreover, the nuclear accumulation of HDAC4

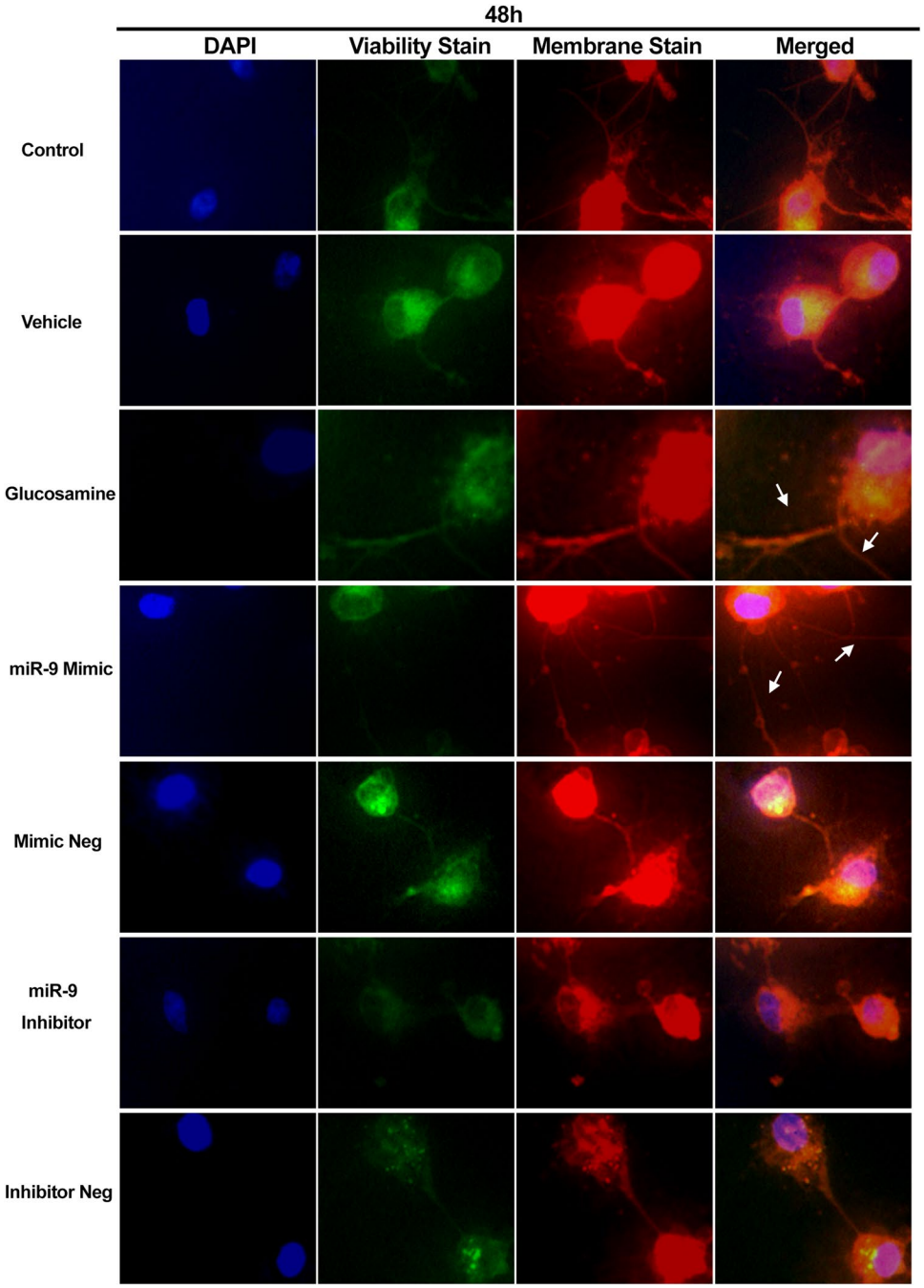

Fig. 11 Neurite outgrowth 48-h post-OGD/R. The fluorescent images demonstrate neurite outgrowth in miR-9/glucosamine-treated cells exposed to OGD after 48 h of reoxygenation (40 ×). The cells are stained with DAPI (blue), viability stain (green), and cell membrane stain (red)

causes neuronal apoptosis while its inactivation attenuates neuronal death (Bolger and Yao 2005). Thus, the consequent HDAC4 inactivation by miR-9 mimic/glucosamine might have contributed to the reduced neuronal death following ischemia.

The significance of miR-9 upregulation in neuronal regeneration was verified by evaluating neuronal proliferation and differentiation, which was compared with the outcome corresponding to glucosamine treatment following ischemia. We observed a precocious increase in neuronal proliferation in miR-9 mimic transfected as well as glucosamine-treated group after OGD/R (Fig. 9). Loss of miR-9 has reportedly retarded the proliferation of human and rat neural progenitor cells (Delaloy et al. 2010). Furthermore, we showed that miR-9 mimic transfection enhanced neurite length at 24-h and 48-h post-OGD, where the effect was concomitant in cells treated with glucosamine (Figs. 10, 11, 12). The increase in neurite length might be associated with the inactivation of HDAC4 and the upregulation of miR-9. A recent study showed that the amassing nuclear HDAC4 is associated with a stark reduction in the length and complexity of neuronal dendrites (Litke et al. 2018). Moreover, HDAC4 inhibition is reported to restore neurite outgrowth, while non-specific HDAC inhibitors such as valproic acid (VPA) and trichostatin A (TSA) promote neurogenesis, neurite outgrowth, and neuroprotection (Trazzi et al. 2016; Hasan et al. 2013).

To further delineate the neuroprotective and regenerative mechanism of glucosamine treatment and miR-9 mimic transfection in ischemic stroke, we quantified the expression of genes closely associated with the ischemic stroke pathology. miR-9 mimic transfection and glucosamine treatment increased BCL2 and VEGF, whereas reduced NFκB1, TNF-α, iNOS, IL-1β mRNA levels following 6-h OGD/R, indicating their decisive role in neuronal survival and regeneration (Fig. 13). BCL2 overexpression is known to impede ischemic stroke-induced neuronal death (Zhao et al. 2003), where miR-9 upregulation reportedly increases BCL2 expression resulting in increased cellular proliferation and reduced apoptosis (Wang et al. 2015). Conversely, NFκB1 activation occurs as an acute response to ischemic injury controlling the production of pro-inflammatory mediators, such as TNF-α, IL-1β, and iNOS, causing inflammation and neuronal death (Harari and Liao 2010; Qian et al. 2017). miR-9 suppresses NFκB1 expression to regulate innate inflammatory responses (Qian et al. 2017; Bazzoni et al. 2009). Moreover, miR-9 diminished local/systemic inflammatory response and promoted pancreatic regeneration *via* the suppressed NFκB1 parallel with the reduced expression of TNF-α and IL-1β (Qian et al. 2017). Overexpression of miR-9 is also reported to significantly attenuate IL-1β–induced TNF-α release in primary osteoarthritis chondrocytes (Jones et al. 2009). Therefore, the reduction of these pro-inflammatory gene levels implies that upregulation of miR-9 might mitigate acute inflammatory responses causing neuronal death following OGD/R.

A significant increase in VEGF expression in miR-9 mimic-transfected and glucosamine-treated cells post-OGD was also observed (Fig. 11). VEGF generates endogenous brain response such as neuronal survival and neurogenesis, resulting in neurovascular remodeling (Fournier and Duman 2012). miR-9 overexpression has been linked to an increased VEGF level in SUM149 cells (Ma et al. 2010). The miR-9 expression is fine-tuned at different stages of neural development promising an effective neuro-regenerative therapy with controlled proliferation and differentiation of neurons.

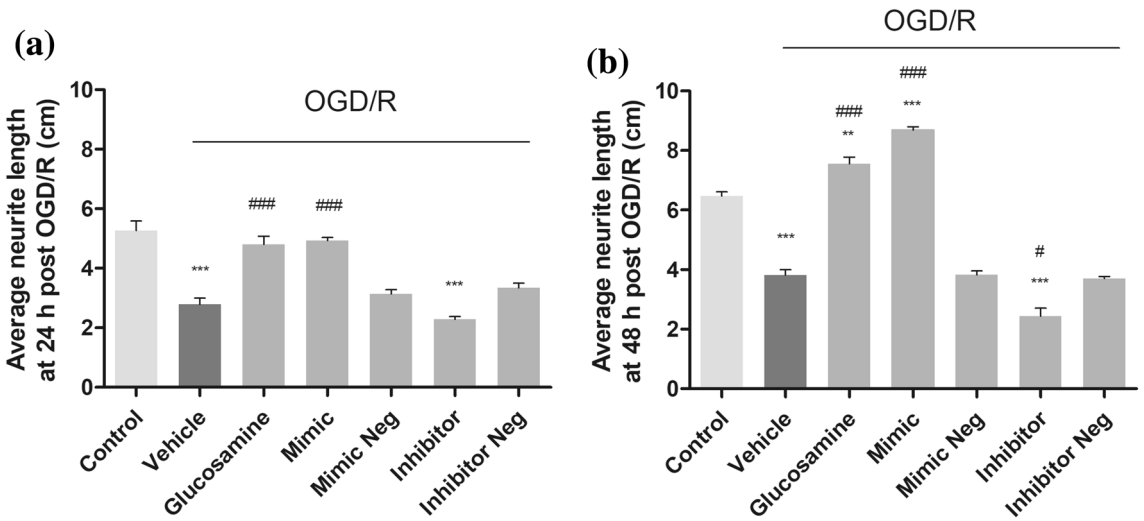

Fig. 12 Quantification of average neurite length. The plot displays the average length of the neurites at **a** 24 h and **b** 48 h of OGD/R. Error bars indicate SEM and $^{***}p < 0.001$, $^{**}p < 0.01$ versus control and $^{\#}p < 0.05$, $^{\#\#}p < 0.01$, $^{\#\#\#}p < 0.001$ versus vehicle

Numerous reports support the use of SH-SY5Y cell line as a suitable in-vitro model to study neurological disorders and to monitor chief cellular events associated with neurodevelopment, including neuronal growth and differentiation (Fordel et al. 2007; Jämsä et al. 2004; Xicoy et al. 2017; Krishna et al. 2014; Radio and Mundy 2008; Kim et al. 1997). It has been widely used to evaluate efficacies of various neuroprotective agents and their mechanism of action, with reproducible outcomes in ex-vivo and in-vivo ischemic stroke models (Sinoy et al. 2017; Chang et al. 2008; Iwashita et al. 2007). SH-SY5Y cell line also offers multiple advantages over a primary neuronal culture that makes it an attractive model to study neuroregeneration mechanisms. It provides a homogenous population of cells, divides rapidly producing a large number of cells in a short period, forms functional synapses, and allows extrinsic regulation of

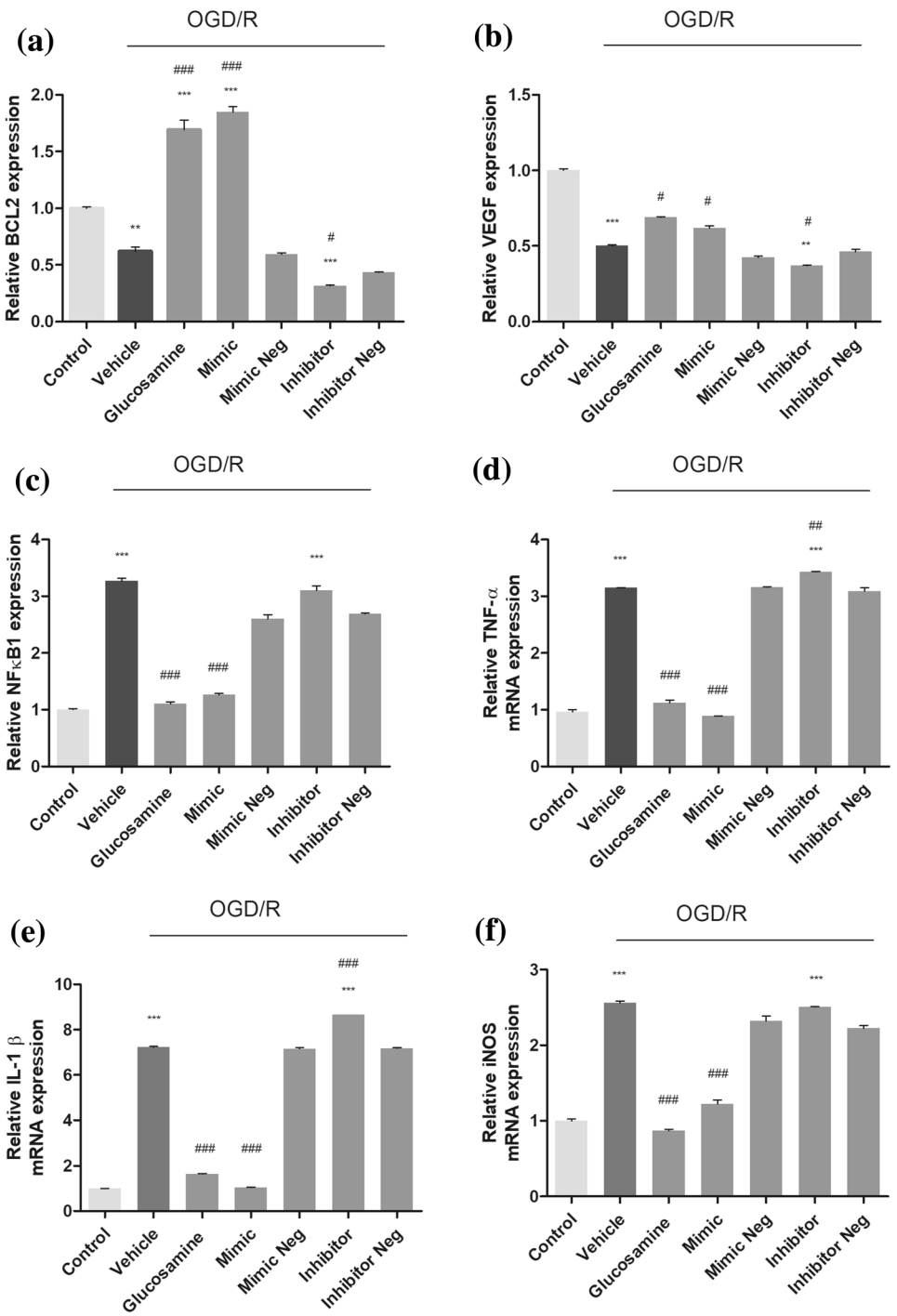

Fig. 13 mRNA expression analysis using qRT-PCR. The graphs depict the fold change in the expression of **a** BCL2 **b** VEGF **c** NFκB1 **d** TNF-α **e** IL-1β, and **f** iNOS in miR-9-transfected and glucosamine-treated cells exposed to OGD/R. Error bars indicate SEM and $^{***}p<0.001$, $^{**}p<0.01$ versus control and $^{\#}p<0.05$, $^{\#\#}p<0.01$, $^{\#\#\#}p<0.001$ versus vehicle

neuronal differentiation. However, these cells may not necessarily display the phenotype of the primary neuronal cell, and the mechanistic basis of neuronal differentiation may be constrained. Despite its limitations, SH-SY5Y cells have still proven to be useful in elucidating fundamental biological processes involved in neuronal differentiation and delineating the effects of exogenous agents on neurite outgrowth.

To recapitulate, our study provides evidence for the first time that miR-9 upregulation is conducive to neuronal survival and regeneration following ischemic stroke. Our findings establish a fundamental mechanism, where HDAC4 inactivation positively regulates miR-9 expression and alleviates ischemic injury in vitro. Importantly, the seminal drug repurposing strategy implemented in this study for miR-9 upregulation might aid in overcoming the challenges that have jeopardized the use of miRNA-based therapies for ischemic stroke.

Acknowledgements This study was funded by (a) the Department of Biotechnology, Government of India "Bioinformatics Infrastructure Facility for Biology Teaching through Bioinformatics (BIFBTBI)" (Grant Number: BT/BI/25/001/2006 dated 25/03/2011) and (b) Kerala State Council for Science, Technology and Environment, Science Research Scheme (Grant Number: 018/SRSLS/2014/CSTE).

Author Contributions SSN and RGK designed experiments; SSN performed experiments, analyzed data, wrote the manuscript; RGK revised the manuscript critically and approved the final version to be submitted.

Compliance with Ethical Standards

Conflict of interest The authors declare no conflict of interest.

Ethical Approval This article does not contain any studies with human participants or animals performed by any of the authors.

References

Ashburn TT, Thor KB (2004) Drug repositioning: identifying and developing new uses for existing drugs. Nat Rev Drug Discov 3:673–683

Bazzoni F, Rossato M, Fabbri M, Gaudiosi D, Mirolo M, Mori L, Tamassia N, Mantovani A, Cassatella MA, Locati M (2009) Induction and regulatory function of miR-9 in human monocytes and neutrophils exposed to proinflammatory signals. Proc Natl Acad Sci USA 106:5282–5287

Bolger TA, Yao TP (2005) Intracellular trafficking of histone deacetylase 4 regulates neuronal cell death. J Neurosci 25:9544–9553

Bottomley MJ, Lo Surdo P, Di Giovine P, Cirillo A, Scarpelli R, Ferrigno F, Jones P, Neddermann P, De Francesco R, Steinkühler C, Gallinari P, Carfí A (2008) Structural and functional analysis of the human HDAC4 catalytic domain reveals a regulatory structural zinc-binding domain. J Biol Chem 283:26694–26704

Chami L, Checler F (2012) BACE1 is at the crossroad of a toxic vicious cycle involving cellular stress and β-amyloid production in Alzheimer's disease. Mol Neurodegener 7:52

Chang R, Algird A, Bau C, Rathbone MP, Jiang S (2008) Neuroprotective effects of guanosine on stroke models in vitro and in vivo. Neurosci Lett 431:101–105

Chen S, Wang M, Yang H, Mao L, He Q, Jin H, Ye ZM, Luo XY, Xia YP, Hu B (2017) LncRNA TUG1 sponges microRNA-9 to promote neurons apoptosis by up-regulated Bcl2l11 under ischemia. Biochem Biophys Res Commun 485:167–173

Coolen M, Katz S, Bally-Cuif L (2013) miR-9: a versatile regulator of neurogenesis. Front Cell Neurosci 7:220

Cramer SC (2018) Treatments to promote neural repair after stroke. J Stroke 20:57–70

Davila JL, Goff LA, Ricupero CL, Camarillo C, Oni EN, Swerdel MR, Toro-Ramos AJ, Li J, Hart RP (2014) A positive feedback mechanism that regulates expression of miR-9 during neurogenesis. PLoS ONE 9:e94348

Davis CK, Nampoothiri SS, Rajanikant GK (2018) Folic acid exerts post-ischemic neuroprotection in vitro through HIF-1α stabilization. Mol Neurobiol 55(11):8328

Delaloy C, Liu L, Lee JA, Su H, Shen F, Yang GY, Young WL, Ivey KN, Gao FB (2010) MicroRNA-9 coordinates proliferation and migration of human embryonic stem cell–derived neural progenitors. Cell stem cell 6:323–335

Dror RO, Dirks RM, Grossman JP, Xu H, Shaw DE (2012) Biomolecular simulation: a computational microscope for molecular biology. Annu Rev Biophys 41:429–452

Fayaz SM, Rajanikant GK (2014) Ensemble pharmacophore meets ensemble docking: a novel screening strategy for the identification of RIPK1 inhibitors. J Comput Aided Mol Des 28:779–794

Fordel E, Thijs L, Martinet W, Schrijvers D, Moens L, Dewilde S (2007) Anoxia or oxygen and glucose deprivation in SH-SY5Y cells: a step closer to the unraveling of neuroglobin and cytoglobin functions. Gene 398:114–122

Fournier NM, Duman RS (2012) Role of vascular endothelial growth factor in adult hippocampal neurogenesis: implications for the pathophysiology and treatment of depression. Behav Brain Res 227:440–449

Guglielmotto M, Aragno M, Autelli R, Giliberto L, Novo E, Colombatto S, Danni O, Parola M, Smith MA, Perry G, Tamagno E, Tabaton M (2009) The up-regulation of BACE1 mediated by hypoxia and ischemic injury: role of oxidative stress and HIF1alpha. J Neurochem 108:1045–1056

Gumireddy K, Young DD, Xiong X, Hogenesch JB, Huang Q, Deiters A (2008) Small-molecule inhibitors of microrna miR-21 function. Angew Chem Int Ed Engl 47:7482–7484

Harari OA, Liao JK (2010) NF-κB and innate immunity in ischemic stroke. Ann N Y Acad Sci 1207:32–40

Hasan MR, Kim JH, Kim YJ, Kwon KJ, Shin CY, Kim HY, Han SH, Choi DH, Lee J (2013) Effect of HDAC inhibitors on neuroprotection and neurite outgrowth in primary rat cortical neurons following ischemic insult. Neurochem Res 38:1921–1934

Hawkins M, Barzilai N, Liu R, Hu M, Chen W, Rossetti L (1997) Role of the glucosamine pathway in fat-induced insulin resistance. J Clin Invest 99:2173–2182

Hwang SY, Shin JH, Hwang JS, Kim SY, Shin JA, Oh ES, Oh S, Kim JB, Lee JK, Han IO (2010) Glucosamine exerts a neuroprotective effect via suppression of inflammation in rat brain ischemia/reperfusion injury. Glia 58:1881–1892

Iwashita A, Muramatsu Y, Yamazaki T, Muramoto M, Kita Y, Yamazaki S, Mihara K, Moriguchi A, Matsuoka N (2007) Neuroprotective efficacy of the peroxisome proliferator-activated receptor delta-selective agonists in vitro and in vivo. J Pharmacol Exp Ther 320:1087–1096

Jämsä A, Hasslund K, Cowburn RF, Bäckström A, Vasänge M (2004) The retinoic acid and brain-derived neurotrophic factor differentiated SH-SY5Y cell line as a model for Alzheimer's

disease-like tau phosphorylation. Biochem Biophys Res Commun 319:993–1000
Jones SW, Watkins G, Le Good N, Roberts S, Murphy CL, Brockbank SM, Needham MR, Read SJ, Newham P (2009) The identification of differentially expressed microRNA in osteoarthritic tissue that modulate the production of TNF-alpha and MMP13. Osteoarthritis Cartilage 17:464–472
Khoshnam SE, Winlow W, Farbood Y, Moghaddam HF, Farzaneh M (2017) Emerging roles of microRNAs in ischemic stroke: as possible therapeutic agents. J Stroke 19:166–187
Kim B, Leventhal PS, Saltiel AR, Feldman EL (1997) Insulin-like growth factor-I-mediated neurite outgrowth in vitro requires mitogen-activated protein kinase activation. J Biol Chem 272:21268–21273
Krishna A, Biryukov M, Trefois C, Antony PM, Hussong R, Lin J, Heinäniemi M, Glusman G, Köglsberger S, Boyd O, van den Berg BH, Linke D, Huang D, Wang K, Hood L, Tholey A, Schneider R, Galas DJ, Balling R, May P (2014) Systems genomics evaluation of the SH-SY5Y neuroblastoma cell line as a model for Parkinson's disease. BMC Genom 15:1154
Laird FM, Cai H, Savonenko AV, Farah MH, He K, Melnikova T, Wen H, Chiang HC, Xu G, Koliatsos VE, Borchelt DR, Price DL, Lee HK, Wong PC (2005) BACE1, a major determinant of selective vulnerability of the brain to amyloid-beta amyloidogenesis, is essential for cognitive, emotional, and synaptic functions. J Neurosci 25:11693–11709
Lang M-F, Shi Y (2012) Dynamic roles of microRNAs in neurogenesis. Front Neurosci 6:71
Langley B, Brochier C, Rivieccio MA (2009) Targeting histone deacetylases as a multifaceted approach to treat the diverse outcomes of stroke. Stroke 40:2899–2905
Lee SY, Lee S, Choi E, Ham O, Lee CY, Lee J, Seo HH, Cha MJ, Mun B, Lee Y, Yoon C, Hwang KC (2018) Small molecule-mediated up-regulation of microRNA targeting a key cell death modulator BNIP3 improves cardiac function following ischemic injury. Sci Rep 8:46973
Litke C, Bading H, Mauceri D (2018) Histone deacetylase 4 shapes neuronal morphology via a mechanism involving regulation of expression of vascular endothelial growth factor D. J Biol Chem 293:8196–8207
Liu XS, Chopp M, Zhang RL, Tao T, Wang XL, Kassis H, Hozeska-Solgot A, Zhang L, Chen C, Zhang ZG (2011) MicroRNA profiling in subventricular zone after stroke: MiR-124a regulates proliferation of neural progenitor cells through Notch signaling pathway. PLoS ONE 6:e23461
Liu XS, Chopp M, Wang XL, Zhang L, Hozeska-Solgot A, Tang T, Kassis H, Zhang RL, Chen C, Xu J, Zhang ZG (2013a) MicroRNA-17-92 cluster mediates the proliferation and survival of neural progenitor cells after stroke. J Biol Chem 288:12478–12488
Liu XS, Chopp M, Zhang RL, Zhang ZG (2013b) MicroRNAs in cerebral ischemia-induced neurogenesis. J Neuropathol Exp Neurol 72:718–722
Ma L, Young J, Prabhala H, Pan E, Mestdagh P, Muth D, Teruya-Feldstein J, Reinhardt F, Onder TT, Valastyan S, Westermann F, Speleman F, Vandesompele J, Weinberg RA (2010) miR-9, a MYC/MYCN-activated microRNA, regulates E-cadherin and cancer metastasis. Nat Cell Biol 12:247–256
Nampoothiri SS, Rajanikant GK (2017) Decoding the ubiquitous role of microRNAs in neurogenesis. Mol Neurobiol 54:2003–2011
Nampoothiri SS, Menon HV, Das D, Krishnamurthy RG (2016) ISCHEMIRs: finding a way through the obstructed cerebral arteries. Curr Drug Targets 17:800–810
Nampoothiri SS, Fayaz SM, Rajanikant GK (2018) A novel five-node feed-forward loop unravels miRNA-Gene-TF regulatory relationships in ischemic stroke. Mol Neurobiol 55(11):8251
Ouyang Y-B, Stary CM, Yang G-Y, Giffard R (2013) microRNAs: innovative targets for cerebral ischemia and stroke. Curr Drug Targets 14:90–101
Pai MY, Lomenick B, Hwang H, Schiestl R, McBride W, Loo JA, Huang J (2015) Drug Affinity Responsive Target Stability (DARTS) for small molecule target identification. Methods Mol Biol 1263:287–298
Pecot CV, Calin GA, Coleman RL, Lopez-Berestein G, Sood AK (2011) RNA interference in the clinic: challenges and future directions. Nat Rev Cancer 11:59–67
Qian D, Wei G, Xu C, He Z, Hua J, Li J, Hu Q, Lin S, Gong J, Meng H, Zhou B, Teng H, Song Z (2017) Bone marrow-derived mesenchymal stem cells (BMSCs) repair acute necrotized pancreatitis by secreting microRNA-9 to target the NF-κB1/p50 gene in rats. Sci Rep 7:581
Radio NM, Mundy WR (2008) Developmental neurotoxicity testing in vitro: models for assessing chemical effects on neurite outgrowth. Neurotoxicology 29:361–376
Shen Q, Temple S (2009) Fine control: microRNA regulation of adult neurogenesis. Nat Neurosci 12:369–370
Shi Y, Zhao X, Hsieh J, Wichterle H, Impey S, Banerjee S, Neveu P, Kosik KS (2010) microRNA regulation of neural stem cells and neurogenesis. J Neurosci 30:14931–14936
Sinoy S, Fayaz SM, Charles KD, Suvanish VK, Kapfhammer JP, Rajanikant GK (2017) Amikacin inhibits miR-497 maturation and exerts post-ischemic neuroprotection. Mol Neurobiol 54:3683–3694
Traxinger RR, Marshall S (1991) Coordinated regulation of glutamine:-fructose-6-phosphate amidotransferase activity by insulin, glucose, and glutamine. Role of hexosamine biosynthesis in enzyme regulation. J Biol Chem 266:10148–10154
Trazzi S, Fuchs C, Viggiano R, De Franceschi M, Valli E, Jedynak P, Hansen FK, Perini G, Rimondini R, Kurz T, Bartesaghi R, Ciani E (2016) HDAC4: a key factor underlying brain developmental alterations in CDKL5 disorder. Hum Mol Genet 25:3887–3907
Wang H, Zhang W, Zuo Y, Ding M, Ke C, Yan R, Zhan H, Liu J, Wang J (2015) miR-9 promotes cell proliferation and inhibits apoptosis by targeting LASS2 in bladder cancer. Tumour Biol 36:9631–9640
Wei N, Xiao L, Xue R, Zhang D, Zhou J, Ren H, Guo S, Xu J (2016) MicroRNA-9 mediates the cell apoptosis by targeting Bcl2l11 in ischemic stroke. Mol Neurobiol 53:6809–6817
Wishart DS, Knox C, Guo AC, Cheng D, Shrivastava S, Tzur D, Gautam B, Hassanali M (2008) DrugBank: a knowledgebase for drugs, drug actions and drug targets. Nucleic Acids Res 36:D901–D906
Xiao Z, Li CH, Chan SL, Xu F, Feng L, Wang Y, Jiang JD, Sung JJ, Cheng CH, Chen Y (2014) A small-molecule modulator of the tumor-suppressor miR34a inhibits the growth of hepatocellular carcinoma. Cancer Res 74:6236–6247
Xicoy H, Wieringa B, Martens GJ (2017) The SH-SY5Y cell line in Parkinson's disease research: a systematic review. Mol Neurodegener 12:10
Xie H, Zhao Y, Zhou Y, Liu L, Liu Y, Wang D, Zhang S, Yang M (2017) MiR-9 regulates the expression of BACE1 in dementia induced by chronic brain hypoperfusion in rats. Cell Physiol Biochem 42:1213–1226
Young DD, Connelly CM, Grohmann C, Deiters A (2010) Small molecule modifiers of microRNA miR-122 function for the treatment of hepatitis C virus infection and hepatocellular carcinoma. J Am Chem Soc 132:7976–7981
Yuan H, Denton K, Liu L, Li XJ, Benashski S, McCullough L, Li J (2016) Nuclear translocation of histone deacetylase 4 induces neuronal death in stroke. Neurobiol Dis 91:182–193
Zhao H, Yenari MA, Cheng D, Sapolsky RM, Steinberg GK (2003) Bcl-2 overexpression protects against neuron loss within the ischemic margin following experimental stroke and inhibits

cytochrome c translocation and caspase-3 activity. J Neurochem 85:1026–1036

Zhao C, Sun G, Li S, Shi Y (2009) A feedback regulatory loop involving microRNA-9 and nuclear receptor TLX in neural stem cell fate determination. Nat Struct Mol Biol 16:365–371

Ziemka-Nalecz M, Zalewska T (2014) Neuroprotective effects of histone deacetylase inhibitors in brain ischemia. Acta Neurobiol Exp (Wars) 74:383–395